

Short Communication

## **Fabrication and Characterization of Pure and Doped Zn/Fe Nanocomposites**

N. M. Deraz<sup>1,2,\*</sup> and A. Alarifi<sup>1</sup>

<sup>1</sup> Catalytic chemistry chair, Chemistry Department, College of Science, King Saud University, Riyadh, Saudi Arabia

<sup>2</sup> Physical Chemistry Department, Laboratory of Surface Chemistry and Catalysis, National Research Center, Dokki, Cairo, Egypt

\*E-mail: [nmderaz@yahoo.com](mailto:nmderaz@yahoo.com)

Received: 16 March 2012 / Accepted: 13 April 2012 / Published: 1 May 2012

---

The goal of this study is to evaluate the influence of the doping by magnesia on the synthesis of zinc/iron nanocomposite. The structural, morphology and magnetic properties of the resulting materials were investigated. The products obtained were characterized by IR, XRD, SEM and VEM techniques. The as synthesized samples show the formation of sponge-like agglomerates. The XRD measurements indicated that pure and doped samples consisted entirely of well crystalline spinel zinc ferrite as a single phase. Magnesia doping led to an increase in both the degree of crystallinity and lattice constant with subsequent a decrease in the density of the investigated solids. The average crystallite size and saturation magnetization were 53 nm and 59 emu/g, respectively, for the sample containing 4mol% MgO. Magnesia doped zinc ferrite showed better magnetic properties for application as soft magnetic devices.

---

**Keywords:** IR; XRD; SEM;  $M_s$ ;  $H_c$ ; MgO-doping

### **1. INTRODUCTION**

The zinc–iron oxides have a spinel structure  $AB_2O_4$  with a tetrahedral A site occupied by  $Zn^{2+}$  ions and an octahedral B site by  $Fe^{3+}$  ions. Based on the distribution of cations, spinels can be either normal like zinc spinel or inverse with half of the trivalent ions in the tetrahedral position and the other half together with the divalent ions in the octahedral sites [1].

Researches carried out in last years over applications of transition metal mixed oxides have shown a high catalytic activity of zinc–iron oxides. The zinc ferrite can be successfully used in processes of hydrocarbons combustion [2]. These oxides have also occurred to be a good catalyst in

reduction of nitrogen oxides in propane–butane mixture [3]. The zinc ferrite's ability to absorb visible light and excellent photochemical stability allowed Zhihao and Lide [4] to find out, that these oxides can be used as a photo-catalyst in photo-induced electron transport and in photo-chemical hydrogen production by photo-catalytic water fission. Valenzuela et al. [5] used zinc ferrite spinel as a photo-catalyst of phenol degradation under ultraviolet radiation.  $\text{ZnFe}_2\text{O}_4$  is considered as attractive gas sensors for reducing gases like liquefied petroleum gas, ethanol, CO and  $\text{CH}_4$  [6]. Also, Zn ferrite is of particular interest as a result of the important role that it plays as an absorbent in the hot gas desulphurisation process [7, 8] and its use in providing scope for mixed ferrites of purpose designed magnetic parameters [9].

The crystalline and magnetic properties of polycrystalline zinc ferrite have been intensively studied because of their high permeability in the radio frequency region. The magnetic characteristics are sensitive to composition, as well as to the synthesis route and grain size [10].

The present work is focused on the properties of a series of pure and magnesia doped zinc/iron nanocomposites obtained via combustion route. The X-ray powder diffraction patterns, the microstructure and the magnetic properties of the as prepared composites are discussed as a function of the magnesia content.

## 2. EXPERIMENTAL

### 2.1. Materials

Undoped and MgO-doped  $\text{ZnFe}_2\text{O}_4$  samples were prepared by mixing calculated proportions of zinc and iron nitrates with a certain amount of glycine and also different amounts of magnesium nitrate. The mixed precursors were concentrated in a porcelain crucible on a hot plate at 250 °C for 5 minutes. The crystal water was gradually vaporized during heating and when a crucible temperature was reached, a great deal of foams produced and spark appeared at one corner which spread through the mass, yielding a voluminous and fluffy product in the container. The as-synthesized products were heat treated at 600 °C for 1 h to enhance their crystallinity and remove the residual charred organic materials. In our experiments, the ratio of the glycine: zinc and ferric nitrates was 1.33. The concentrations of magnesium expressed as mol% MgO were 1, 2 and 4. The chemicals employed in the present work were of analytical grade supplied by Prolabo Company.

### 2.2. Techniques

An X-ray measurement of various mixed solids was carried out using a BRUKER D8 advance diffractometer. The patterns were run with  $\text{Cu K}_\alpha$  radiation at 40 kV and 40 mA with scanning speed in  $2\theta$  of  $2^\circ \text{ min}^{-1}$ .

The crystallite size of Zn-ferrite present in the investigated solids was based on X-ray diffraction line broadening and calculated by using Scherrer equation [11].

$$d = \frac{B\lambda}{\beta \cos \theta} \quad (1)$$

An infrared transmission spectrum of various solids was determined using Perkin-Elmer Spectrophotometer (type 1430). The IR spectra were determined from 900 to 300  $\text{cm}^{-1}$ . Two mg of each solid sample were mixed with 200 mg of vacuum-dried IR-grade KBr. The mixture was dispersed by grinding for 3 min in a vibratory ball mill and placed in a steel die 13 mm in diameter and subjected to a pressure of 12 tonnes. The sample disks were placed in the holder of the double grating IR spectrometer.

Scanning electron micrographs (SEM) were recorded on JEOL JAX-840A electron microanalyzers, respectively. The samples were dispersed in ethanol and then treated ultrasonically in order to disperse individual particles over a gold grid.

The magnetic properties of the investigated solids were measured at room temperature using a vibrating sample magnetometer (VSM; 9600-1 LDJ, USA) in a maximum applied field of 15 kOe. From the obtained hysteresis loops, the saturation magnetization ( $M_s$ ), remanence magnetization ( $M_r$ ) and coercivity ( $H_c$ ) were determined.

### 3. RESULTS AND DISCUSSION

The FTIR spectra for the pure and magnesia doped zinc/iron system were recorded in the range 300–900  $\text{cm}^{-1}$ , which is shown in Fig.1.

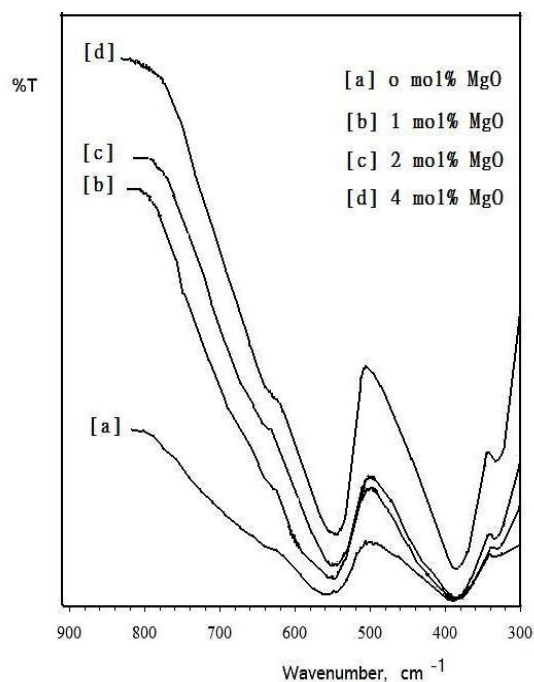


**Figure 1.** FTIR spectra of Zn/Fe composite treated with different amounts of magnesium oxide.

The spectra show two main absorption bands  $\nu_1$  and  $\nu_2$  corresponding to the stretching vibration of the tetrahedral and octahedral sites around  $390$  and  $550\text{ cm}^{-1}$ , respectively, are responsible for the formation of  $\text{ZnFe}_2\text{O}_4$  [12]. The band  $\nu_2$  at  $390\text{ cm}^{-1}$  has a subsidiary band  $\nu_2^*$  at  $325\text{ cm}^{-1}$ . This subsidiary may be due to the Jahn–Teller distortion produced by  $\text{Fe}^{2+}$  ions [13]. However, the existence of a weak shoulder,  $\nu_1^*$ , around the  $\nu_1$  band at  $625\text{ cm}^{-1}$  indicating the presence of zinc ion. In addition, the average value of the threshold energy is  $0.095\text{ eV}$ . The spectra also show a change in the position and intensity of absorption bands due to the introduction of  $\text{Mg}^{2+}$  ions. This can be attributed to redistribution of cations between tetrahedral and octahedral sites due to  $\text{MgO}$ -doping [14]. The crystalline bulk form of  $\text{ZnFe}_2\text{O}_4$  is a normal spinel with  $\text{Zn}^{2+}$  ions only on the A sites and  $\text{Fe}^{3+}$  ions only on the B sites. Recent investigations of nanocrystalline  $\text{ZnFe}_2\text{O}_4$  have suggested that the cation distribution in this material is partly inverted and exhibits anomaly in its magnetization [12].

Fig. 2 represents the X-ray powder diffraction patterns of synthesized samples. All the samples can be indexed as the single-phase cubic spinel structure.

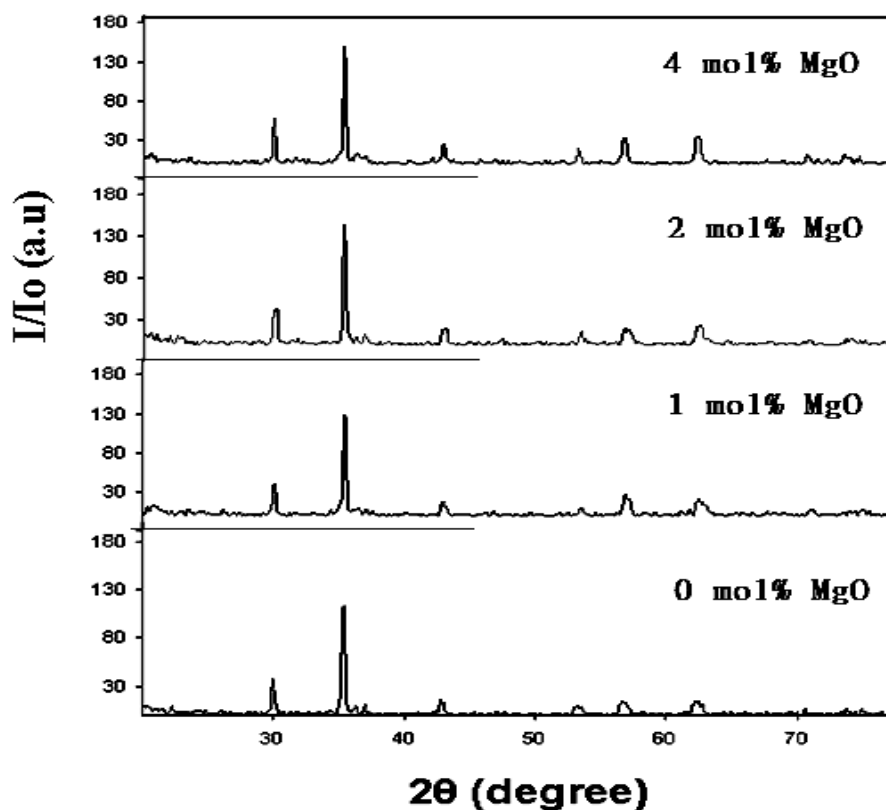


**Figure 2.** X-ray diffraction patterns of Zn/Fe composite treated with different amounts of magnesium oxide.

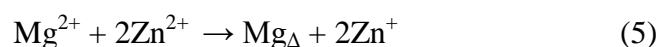
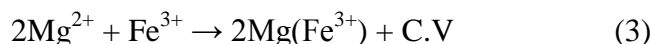
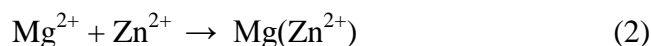
The calculated crystallite size ( $d$ ), lattice constant ( $a$ ), unit cell volume ( $V$ ) and X-ray density ( $D_x$ ) values are listed in Table 1.

**Table 1.** The effects of MgO- doping on some structural parameters of zinc ferrite.

| Concentration of MgO (mol %) | d (nm) | a (nm) | V (nm <sup>-3</sup> ) | D <sub>x</sub> (g/cm <sup>3</sup> ) |
|------------------------------|--------|--------|-----------------------|-------------------------------------|
| 0                            | 45     | 0.8409 | 0.5943                | 5.387                               |
| 1                            | 47     | 0.8412 | 0.5952                | 5.380                               |
| 2                            | 49     | 0.8420 | 0.5969                | 5.367                               |
| 4                            | 53     | 0.8425 | 0.5980                | 5.357                               |

It can be seen from this table that MgO-doping led to an increase in the a, D and V values of zinc ferrite system due to the difference in ionic radii ( $Zn^{2+}=0.074$  nm,  $Mg^{2+}=0.066$  nm,  $Fe^{3+}=0.064$ nm). However, this treatment brought about a decrease in the D<sub>x</sub> value of ZnFe<sub>2</sub>O<sub>4</sub> nanoparticles due to the fact that both density and the atomic concentration of Mg atom are lower than that of Zn atom [15].

Magnesium oxide dopant could be dissolved in the lattices of each reacting oxides involved in the forming zinc ferrite. The dissolution process can be can be simplified by the use of Kröger's notations [16] in the following manner:

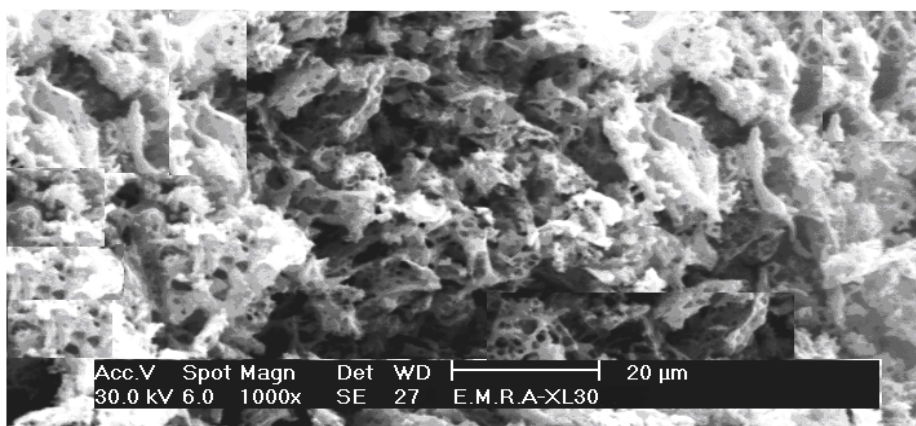


$Mg(Zn^{2+})$  and  $Mg(Fe^{3+})$  are the divalent lithium ions located in the positions of host zinc and iron oxides in ZnO and Fe<sub>2</sub>O<sub>3</sub>, respectively;  $Mg_{\Delta}$  is magnesium ions located in the interstitial positions of zinc and ferric oxide lattices; C.V. created cationic vacancies.

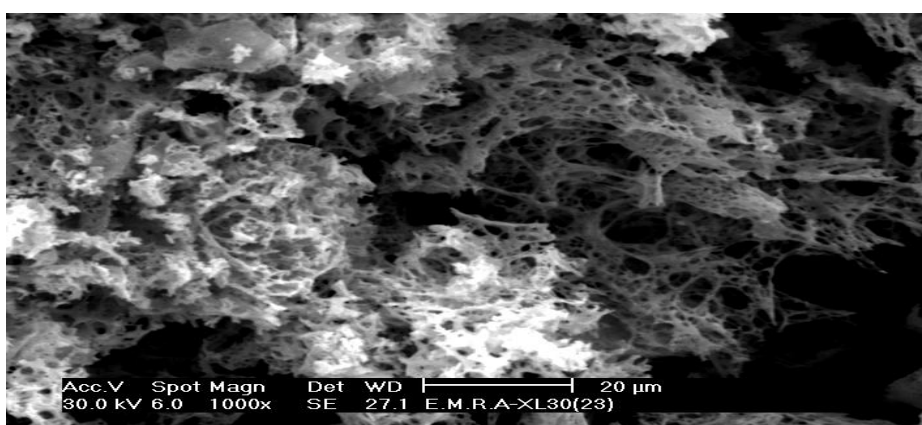
The dissolution of dopant ions in the lattices of reacting oxides according to reaction (3) which led to creation of cationic vacancies might increase the mobility of cations of reacting oxides thus enhancing the ferrite formation.

Incorporation of magnesium ions in Fe<sub>2</sub>O<sub>3</sub> and ZnO lattices according to reactions (4) and (5) decreased the number of reacting cations ( $Zn^{2+}$  and  $Fe^{3+}$ ) involved in the ferrite formation. So, reaction (3) might be expected to stimulate zinc ferrite formation, while reactions (4) and (5) might exert an opposite effect. The fact that MgO-doping of Zn/Fe oxides system enhanced zinc ferrite formation suggesting the domination of reaction (3).

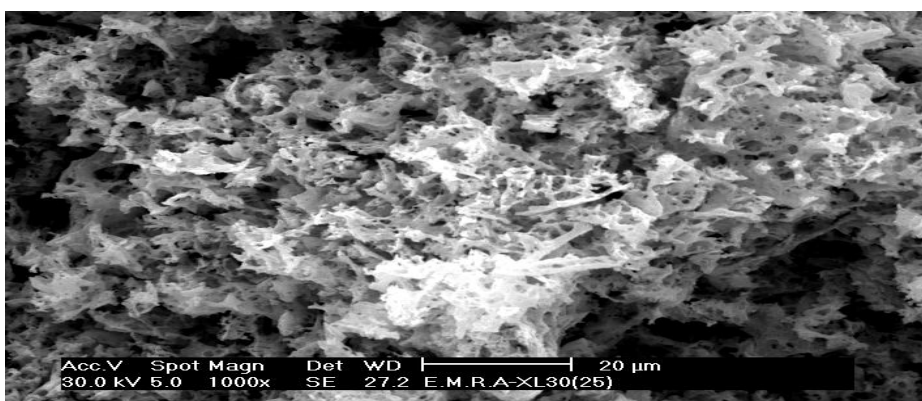
Fig. 3a–c depicts the scanning electron, SEM, micrographs of the pure and doped zinc/ iron composite samples.



A



B



C

**Figure 3.** SEM images for pure Zn/Fe composite sample (a) and those treated with 2 mol% MgO (b) and 4 mol% MgO (c).

These micrographs reflect agglomerated, well-defined particles with inhomogeneous grain size distribution due to magnesia doping [17]. The preparation of the investigated solids by combustion process resulted in the formation of spongy and fragile network structure containing voids and pores due to the release of large amount gases. Also, SEM micrographs of the sample treated with 4 mol% MgO (Fig. 3c) show fracture surfaces of the powders.

The magnetization curves of pure and doped Zn/Fe composites, obtained from room temperature VSM measurements. From VSM measurements, the magnetization and the coercivity are derived and tabulated in Table 2.

**Table 2.** The effects of magnesia doping on the magnetic properties ( $M_s$ ,  $M_r$  and  $H_c$ ) of the as-prepared solids.

| Concentration of MgO (mol %) | $M_s$ (emu/g) | $M_r$ (emu/g) | $M_r/M_s$ (emu/g) | $H_c$ (Oe) |
|------------------------------|---------------|---------------|-------------------|------------|
| 0                            | 52            | 14            | 0.269             | 46         |
| 1                            | 54            | 15            | 0.278             | 46         |
| 2                            | 57            | 15            | 0.263             | 45         |
| 4                            | 59            | 16            | 0.271             | 41         |

It can be seen from this table that the doping with MgO brought about an increase in the magnetization of zinc ferrite nanoparticles. This treatment resulted in a decrease in the coercivity of the investigated ferrite. It is well known that nano-sized particles have small domain areas whose boundaries or domain walls prevent their rotation and/or spin, contributing to reduce their magnetization. Thus, in this work, the powder particles treated with magnesia were approximately 17.8% larger than undoped sample, contributing directly to increase magnetization due to their larger domain area. Therefore, the larger particle size of the 4 mol% MgO-doped zinc ferrite powders showed saturation magnetization values of 59emu/g.

#### 4. CONCLUSIONS

Combustion reaction synthesis using glycine as fuel led to the formation of monophasic crystalline  $ZnFe_2O_4$  powders. The average crystallite size of the powders synthesized with was 45-53 nm. All the as synthesized samples show the formation of sponge-like agglomerates with pre-sintered secondary particles of irregular morphology. The samples synthesized with magnesia presented superior magnetic characteristics.

#### ACKNOWLEDGEMENT

This work was supported by NPST program by King Saud University Project: Number 09-ADV651-02.

#### References

1. Guoying Zhang, Chunsheng Li, Fangyi Cheng, Jun Chen, *Sensors and Actuators B* 120 (2007) 403

2. S. Kumar, A.M.M. Farea, K.M. Batoo, C.G. Lee, B.H. Koo, A. Yousef, Alimuddin, *Physica B* 403 (2008)3604.
3. K.S. Gavrilenko, T.V. Mironyuk, V.G. Il'in, S.N. Orlik, V.V. Pavlishchuk, *Theor. Exp. Chem.* 38 (2002) 118.
4. Y. Zhihao, Z. Lide, *Mater. Res. Bull.* 33 (1998) 1587.
5. M.A. Valenzuela, P. Bosch, J. Jimenez-Becerrill, O. Quiroz, A.I. Páez, *J. Photochem. Photobiol. A: Chem.* 148 (2002) 177.
6. S.V. Manorama, L. Satyanarayana, K. Madhusudan-Reddy, *Sensors Actuators B Chem.* 89 (2003) 62.
7. S.K. Gangwal, J.M. Stogner, S.M. Harkins, S.J. Bossart, *Environ. Prog.* 8(1989)26
8. M. Ahmed, L. Alonso, J.M. Palacios, C. Cilleruelo, J.C. Abanades, *Solid State Ionics* 138 (2000) 51.
9. H.H. Hamdeh, J.C. Ho, S.A. Oliver, R.J. Willey, G. Oliveri, G. Busca, *J. Appl. Phys.* 81 (1997) 1851.
10. Mona Mouallem-Bahout, Sarah Bertrand, Octavio Peña, *Journal of Solid State Chemistry* 178 (2005) 1080.
11. B.D. Cullity, *Elements of X-ray Diffraction*, Addison-Wesley Publishing Co. Inc. 1976 (Chapter 14).
12. N.M. Deraz, A. Alarifi, *Polyhedron* 28 (2009) 4122.
13. V.A. Potakova, N.D. Zverv, V.P. Romanov, *Phys. Stat. Sol. (a)* 12 (1972) 623.
14. S.C. Watawe, B.D. Sutar, B.D. Sarwade, B.K. Chougule, *Int. J. Inorg. Mater.* 3 (2001) 819.
15. L. John Berchmans, R. Kalai Selvan, P.N. Selva Kumar, C.O. Augustin, *J. Magn. Magn. Mater.* 279 (2004) 103.
16. F.A. Kröger, *Chemistry of Imperfect Crystals*, North-Holland, Amsterdam, 1964.
17. A. Alarifi, N. M. Deraz and S. Shaban, *J. Alloy Compds* 486 (2009) 501.